The role of Carbon and C-H neutralization in MOCVD β-Ga₂O₃ using TMGa as precursor

Lingyu Meng¹, A F M Anhar Uddin Bhuiyan¹, and Hongping Zhao^{1,2,‡}

¹Department of Electrical and Computer Engineering, The Ohio State University, Columbus, OH 43210, USA

²Department of Materials Science and Engineering, The Ohio State University, Columbus, OH 43210, USA

‡Corresponding Email: <u>zhao.2592@osu.edu</u>

Abstract

In this letter, the role of background carbon in metalorganic chemical vapor deposition (MOCVD) β-Ga₂O₃ growth using trimethylgallium (TMGa) as the Ga precursor was investigated. The quantitative C and H incorporations in MOCVD β-Ga₂O₃ thin films grown at different growth rate and temperature were measured via quantitative secondary ion mass spectroscopy (SIMS). The SIMS results revealed both [C] and [H] increase as the TMGa molar flow rate/growth rate increases or growth temperature decreases. The intentional Si incorporation in MOCVD β-Ga₂O₃ thin films decreases as the growth rate increases or the growth temperature decreases. For films grown at relatively fast growth rates (GR) (TMGa>58 µmol/min, GR>2.8 µm/h) or relatively low temperature (<950 °C), the [C] increases faster than that of the [H]. The experimental results from this study demonstrate the previously predicted theory - H can effectively passivate the compensation effect of C in n-type β-Ga₂O₃. The extracted net doping concentration from quantitative SIMS ([Si]-([C]-[H])) agrees well with the free carrier concentration measured from Hall measurement. The revealing of the role of C compensation in MOCVD β-Ga₂O₃ and effect of H incorporation will provide guidance on designing material synthesis for targeted device applications.

Keywords: Ultrawide bandgap semiconductor, β-Ga₂O₃, MOCVD, background carbon

β-Ga₂O₃ has been considered as a promising semiconductor candidate for high power and radio frequency (RF) electronics because of its ultrawide energy bandgap (4.8 eV) and predicted high critical field strength (8 MV/cm) [1-3]. Yet, the material is n-type dopable with shallow donors and a wide range of doping concentration from 10¹⁶ cm⁻³ to 10²⁰ cm⁻³ [4–8]. The availability of high crystalline quality Ga₂O₃ substrates [9] with different orientations ((010), (100), (001), (-201)) enables high quality epitaxy of β-Ga₂O₃ [5–7, 10–27] and β-AlGaO [28–34]. Several growth methods have been used to develop β-Ga₂O₃ thin films including molecular beam epitaxy (MBE) [6, 11, 35, 36], pulsed laser deposition (PLD) [37–39], halide vapor phase epitaxy (HVPE) [5, 40– 42], low pressure chemical vapor deposition (LPCVD) [8, 14, 43–45] and metalorganic chemical vapor deposition (MOCVD) [4, 7, 16, 17, 23, 25, 46-48]. Among them, MOCVD has been demonstrated to produce high crystalline quality materials with record room temperature and low temperature mobilities that approach the theoretical values [7, 20, 23, 49]. The typical growth rate for MOCVD β-Ga₂O₃ using triethylgallium (TEGa) as the Ga precursor ranges between 0.2-1.0 μm/h [17, 23, 48, 49]. For devices require thick epi-layers such as vertical power devices, epifilms with fast growth rate and high crystalline quality are required. Current device demonstrations on vertical β-Ga₂O₃ Schottky diodes or vertical pn diodes with thick drift layers are mainly based on HVPE grown materials [13, 50-56]. However, due to rough and non-uniform surface morphologies of HVPE grown β-Ga₂O₃ [41], chemical-mechanical polishing process is required for device processing, which can cause impurities incorporation and prevent in-situ epitaxy of heterojunctions.

On the other hand, MOCVD growth of β-Ga₂O₃ using trimethylgallium (TMGa) as the Ga precursor on (010) Ga₂O₃ substrates has been demonstrated with relatively fast growth rate up to

~3 µm/h [25]. Room temperature mobility as high as 190 cm²/Vs with carrier concentration of 1.8 $x10^{16}$ cm⁻³ and compensation level of $\sim 1.5 \times 10^{15}$ cm⁻³ was achieved [25]. Previously, MOCVD growth of (010) β-Ga₂O₃ using TMGa with growth rate of 1.5 μm/h reported room temperature mobility of 125 cm²/Vs with carrier concentration of 1.5 x10¹⁶ cm⁻³, and low temperature peak mobility of 23000 cm²/Vs at 32 K [20]. These results indicate a great potential to develop high quality thick β-Ga₂O₃ films via MOCVD using TMGa as the Ga precursor. As compared to TEGa (3 torr at 20°C), TMGa has a higher vapor pressure (65 torr at 0°C) [57] and a shorter reaction pathway (in contrast to TEGa, which undergoes a three-step decomposition process, TMGa pyrolyzes via a two-step unimolecular reaction, generating monomethylgallium and a methyl group as by-products) [20, 58, 59], which enables faster growth rates of β-Ga₂O₃. Carbon (C) is considered as one of the most common impurities in MOCVD grown materials as it originates from the metalorganic (MO) precursors. Particularly, C incorporation is higher using TMGa as compared to that of the TEGa. TEGa decomposes via β-elimination and has a lower decomposition temperature, thus lowering carbon incorporation into the surface during MOCVD growth [60]. It was well understood that C is one of the main sources of charge compensation in the MOCVD grown n-type GaN [61, 62]. However, the role of C in MOCVD growth of β-Ga₂O₃ is still not well understood.

In this work, C incorporation in MOCVD grown β-Ga₂O₃ on (010) Ga₂O₃ substrates using TMGa as the Ga precursor is systematically studied as a function of the growth rate and growth temperature. TMGa and pure O₂ were used as the precursors of Ga and O, respectively. Argon was used as the carrier gas. Si doping was introduced by using the diluted silane source (diluted with N₂, 25ppm) in the Si-doped samples. The growth pressure was set at 60 Torr and the O₂ flow rate was set at 800 standard cubic centimeter per minute (sccm). The TMGa molar flow rate was varied

between 39 μmol/min and 116 μmol/min. The growth temperature was controlled between 700°C and 950°C. All samples were grown on Fe-doped semi-insulating (010) β-Ga₂O₃ substrates, which were ex-situ cleaned with acetone, IPA, and DI-water prior loading to the growth chamber. Quantitative secondary ion mass spectroscopy (SIMS) was used to probe the impurity profiles of C, hydrogen (H), and silicon (Si). C and H represent the common impurities in MOCVD-grown materials, as they originate from the metalorganic (MO) precursors. Background Si is also a common impurity in MOCVD grown Ga₂O₃, which is from the growth chamber. From our previous studies, the background Si incorporation is highly dependent on the growth pressure [24]. Room temperature carrier transport characteristics were measured via van der Pauw Hall measurement (Ecopia HMS 3000, magnetic field=0.975 T). Ti/Au (30/100 nm) contacts were deposited on the four corners of the sample and annealed at 470 °C under N₂ for 1 min to obtain Ohmic contacts.

The impurity concentrations of C, Si and H, as a function of the TMGa molar flow rate was studied by quantitative SIMS on a multi-layer stack sample (stack I) as shown in Fig. 1(a). The growth temperature was kept at 950 °C. The silane flow rate was set at 0.416 nmol/min in the Sidoped sub-layers, which were sandwiched between the un-intentionally doped (UID) layers. The TMGa molar flow rate was varied from 39 to 116 μmol/min. The SIMS profiles of C, H, and Si remain constant in each sub-layer, suggesting that the diffusion process for C, H, and Si is negligible. Fig. 1(b) shows the SIMS depth profiles of the impurity elements C, H and Si. The detection limit for C, H and Si is 3 x 10¹⁶ cm⁻³, 5 x 10¹⁶ cm⁻³, and 5 x 10¹⁵ cm⁻³, respectively. The β-Ga₂O₃ growth rate under different TMGa flow rate was extracted from the SIMS depth profiles. It increases from 1.3 μm/h to 6.7 μm/h with the TMGa molar flow rate tuned from 39 μmol/min to 116 μmol/min. From Fig. 1(b), an obvious monotonic increase of both [C] and [H] was observed

as the β -Ga₂O₃ growth rate increases. Both [C] and [H] does not show dependence on the Si doping within the sub-layers grown at the same TMGa flow rate. The background Si in the UID sub-layers was below or at the Si SIMS detection limit (5×10^{15} cm⁻³). Fig. 2 plots the [Si], [C] and [H] as a function of the TMGa molar flow rate. As the TMGa flow rate increases, [C] increases at a faster rate as compared to that of [H]. The [C] increases from 4.1 x 10^{16} cm⁻³ to 1.7 x 10^{18} cm⁻³, as the TMGa flow rate increases from 39 µmol/min to 116 µmol/min. The [Si] decreases as the TMGa flow rate increases due to the reduction of Si adatom concentration at the growth surface. On the other hand, the companion increase of [H] with [C] indicates the possibility of C-H complex formation. The increase in H incorporation with the increase of the TMGa molar flow rate strongly suggests that the H impurity originates from the TMGa precursor. It is likely that the H incorporation occurs due to the decomposition of H₂O - a by-product of the chemical reaction between monomethylgallium and O₂. Due to the decomposition of H₂O, it is likely that part of the H reacts with methyl radicals to form stable CH₄., and part of the H react with C forming C-H complexes in Ga₂O₃.

To study the compensation effect from C, a series of samples grown at different growth rates with different silane flow rates were designed for Hall measurements. As shown in Fig. 3, the carrier concentration and electron mobility of three sets of samples with different growth rates (2.8 μ m/h, 5.3 μ m/h and 6.7 μ m/h) were characterized as a function of the silane flow rate. With the tuning of silane flow rate in a wide range, the measurable range of free carrier concentration differs drastically for the three sets of samples. For the samples grown at relatively low TMGa flow rate (58 μ mol/min) or low growth rate (2.8 μ m/h), a wide range of carrier concentration from 1.6 x 10¹⁶ to 3.8 x 10¹⁹ cm⁻³ was measurable. However, as the growth rate increases, the measurable range of carrier concentration becomes narrower. In the case of fast growth rate condition at 6.7 μ m/h, only

samples with high doping concentrations are measurable. Samples grown with low silane flow rates show high resistivity. This trend indicates a strong compensation effect in films grown at fast growth rates with high [C]. By comparing the measured carrier concentration and the corresponding [C], [H] concentrations for each set of samples, we found that the net concentration of [C]-[H] agrees well with the compensation level for each set with different growth rate. As shown in Fig.3, the dash-dot lines ([C]-[H]) plotted based on the quantitative SIMS data, agree well with compensation level for each case with different growth rate. The incorporated H forms C-H complexes and therefore passivates the compensation effect from pure C.

Prior theoretical studies based on the density-function theory (DFT) predicted that C on Ga site (C_{Ga}) acts as a shallow donor in Ga₂O₃ and C on oxygen site (C_O) acts as a compensating acceptor [63]. However, experimental results do not show good agreement with either of these two cases. In our previous studies [25], the temperature dependent Hall measurement of the β-Ga₂O₃ epi-film grown with the TMGa flow rate of 58 μmol/min (growth rate of 2.95 μm/h) revealed an extracted charge compensation level of 1.45×10¹⁵ cm⁻³, while the corresponding SIMS data showed [C] and [H] were at \sim mid- 10^{16} cm⁻³. This shows a strong indication of the passivation effect of H on the C compensation. Recent DFT calculations also show the neutralization of C-H complexes in β-Ga₂O₃ [63]. The strength of C-H bond, which is related to the small atomic size of C, makes the C-H combination behave as a unit, similar to a nitrogen atom, and lowers the overall formation energy. Therefore, for the MOCVD growth of β-Ga₂O₃, the incorporation of both C and H can reduce the net compensation level to [C]-[H]. Particularly, as shown in Fig. 2, with relatively low TMGa flow rate (<58 µmol/min), the [H] is comparable to [C], thus the net compensation level ([C]-[H]) is significantly suppressed, which enables the tunable doping level at low-10¹⁶ cm⁻ ³. As the TMGa flow rate increases (>58 µmol/min), [C] increases faster as compared to [H], which

leads to a strong increase of the net compensation level ([C]-[H]). Thus, the controllable net carrier concentration strongly depends on the growth rate.

The electron mobility as a function of carrier concentration for samples grown with different TMGa flow rates/growth rates is shown in Fig. 3(b). With the same TMGa flow rate/growth rate, the general trend shows that the electron mobility decreases as the carrier concentration increases. For the case with fast growth rate at 6.7 µm/h and strong compensation, the electron mobility does not show obvious dependence on the carrier concentration within the measurable range. With the same carrier concentration, the electron mobility decreases as the growth rate increases. This is likely due to the increased scattering mechanism from the high compensation concentration.

In addition to the growth rate, the growth temperature is expected to affect C incorporation in MOCVD β -Ga₂O₃. In this work, the impurities incorporation as a function of growth temperature were studied with another designed growth stack (stack II), as shown in Fig. 4 (a). The TMGa molar flow rate and chamber pressure were set at 58 μ mol/min and 60 torr, respectively. The silane flow rate was set at 0.416 nmol/min in the Si-doped sub-layers. The growth temperature was varied from 950 °C to 700 °C. The SIMS depth profiles of impurity elements C, H and Si were shown in Fig. 4(b). The detection limit for C, H and Si is 1 x 10¹⁷ cm⁻³, 5 x 10¹⁶ cm⁻³, and 5 x 10¹⁵ cm⁻³, respectively. The growth rate of β -Ga₂O₃ under different growth temperature was estimated from the SIMS depth profiles and was listed in Fig. 4(a). As shown in Fig. 4(b), the C incorporation has a strong dependence on the growth temperature. The [C] increases from ~7 x 10¹⁶ cm⁻³ to 3.5 x 10²¹ cm⁻³ as the growth temperature decreases from 950 °C to 700 °C. Within the same growth temperature range, the [H] increases from 7.0 x 10¹⁶ cm⁻³ to 1.0 x 10¹⁹ cm⁻³. In contrast, [Si] does not show a strong dependence on the growth temperature. The extracted C, H and Si concentrations as a function of the growth temperature was plotted in Fig. 5. Both [C] and

[H] increase as growth temperature decreases, but [C] increases faster as compared to [H]. The faster decrease in carbon impurity incorporation at higher temperatures as compared to that of hydrogen can be attributed to the enhanced H diffusion at higher temperatures. At relatively high growth temperature, the net compensation ([C]-[H]) can be maintained at relatively low level. The slight decrease of [Si] from 950°C to 800°C is mainly due to the slight increase of the corresponding growth rate from 2.7 μm/h to 3.1 μm/h. The lower Si concentration at 700°C is mainly attributed to the lower Si incorporation efficiency at low temperatures.

In conclusion, the role of C on the compensation effect in the MOCVD β -Ga₂O₃ epitaxy using TMGa as the Ga precursor was systematically investigated. The results revealed that both high TMGa flow rate/growth rate and low growth temperature can lead to higher C incorporation. Typically, [H] in MOCVD β -Ga₂O₃ increases with [C], but with a slower increasing rate. The formation of C-H complexes in MOCVD β -Ga₂O₃ results in the passivation of the compensation effect from pure C. The quantitative SIMS and charge transport characteristics revealed that the net compensation effect is determined to be [C]-[H]. Results from this work indicate that (i) the background C incorporation is highly dependent on the MOCVD growth condition; (ii) the [C] can be widely controlled from below C detection limit (\sim 5x10¹⁶ cm⁻³) to as high as mid-10²¹ cm⁻³, indicating a potential effective approach to control the conductivity of the film; and (iii) intentional incorporation of H in MOCVD β -Ga₂O₃ can potentially suppress the compensation level via the passivation of C. These results will provide valuable guidance and flexibility for future device design and development.

Conflict of Interest Statement

On behalf of all authors, the corresponding author states that there is no conflict of interest.

Acknowledgement

The authors thank the financial support from the Air Force Office of Scientific Research FA9550-18-1-0479 (AFOSR, Dr. Ali Sayir) and the NSF (Grant No. 2231026, No. 2019753).

Data Availability

The data that support the findings of this study are available from the corresponding author upon reasonable request.

References:

- [1] H. H. Tippins, Phys. Rev. **140**, A316 (1965).
- [2] T. Onuma, S. Fujioka, T. Yamaguchi, M. Higashiwaki, K. Sasaki, T. Masui, and T. Honda, Appl. Phys. Lett. **103**, 041910 (2013).
- [3] M. Higashiwaki, K. Sasaki, A. Kuramata, T. Masui, and S. Yamakoshi, Appl. Phys. Lett. **100**, 013504 (2012).
- [4] M. Baldini, M. Albrecht, A. Fiedler, K. Irmscher, D. Klimm, R. Schewski, and G. Wagner, J. Mater. Sci. **51**, 3650 (2016).
- [5] K. Goto, K. Konishi, H. Murakami, Y. Kumagai, B. Monemar, M. Higashiwaki, A. Kuramata, and S. Yamakoshi, Thin Solid Films **666**, 182 (2018).
- [6] E. Ahmadi, O. S. Koksaldi, S. W. Kaun, Y. Oshima, D. B. Short, U. K. Mishra, and J. S. Speck, Appl. Phys. Express 10, 041102 (2017).
- [7] Y. Zhang, F. Alema, A. Mauze, O. S. Koksaldi, R. Miller, A. Osinsky, and J. S. Speck, APL Mater. 7, 022506 (2019).
- [8] S. Rafique, L. Han, A. T. Neal, S. Mou, J. Boeckl, and H. Zhao, Phys. Status Solidi A 215, 1700467 (2018).
- [9] A. Kuramata, K. Koshi, S. Watanabe, Y. Yamaoka, T. Masui, and S. Yamakoshi, Jpn. J. Appl. Phys. **55**, 1202A2 (2016).
- [10] K. D. Leedy, K. D. Chabak, V. Vasilyev, D. C. Look, K. Mahalingam, J. L. Brown, A. J. Green, C. T. Bowers, A. Crespo, D. B. Thomson, and G. H. Jessen, APL Mater. 6, 101102 (2018).

- [11] K. Sasaki, A. Kuramata, T. Masui, E. G. Villora, K. Shimamura, and S. Yamakoshi, Appl. Phys. Express **5**, 035502 (2012).
- [12] A. Mauze, Y. Zhang, T. Itoh, E. Ahmadi, and J. S. Speck, Appl. Phys. Lett. 117, 222102 (2020).
- [13] J. H. Leach, K. Udwary, J. Rumsey, G. Dodson, H. Splawn, and K. R. Evans, APL Mater. 7, 022504 (2019).
- [14] Y. Zhang, Z. Feng, M. R. Karim, and H. Zhao, J. Vac. Sci. Technol. A 38, 050806 (2020).
- [15] A. Bhattacharyya, P. Ranga, S. Roy, J. Ogle, L. Whittaker-Brooks, and S. Krishnamoorthy, Appl. Phys. Lett. **117**, 142102 (2020).
- [16] M. Baldini, M. Albrecht, A. Fiedler, K. Irmscher, R. Schewski, and G. Wagner, ECS J. Solid State Sci. Technol. 6, Q3040 (2016).
- [17] S. Bin Anooz, R. Grüneberg, C. Wouters, R. Schewski, M. Albrecht, A. Fiedler, K. Irmscher, Z. Galazka, W. Miller, G. Wagner, J. Schwarzkopf, and A. Popp, Appl. Phys. Lett. 116, 182106 (2020).
- [18] T.-S. Chou, P. Seyidov, S. Bin Anooz, R. Grüneberg, T. T. V. Tran, K. Irmscher, M. Albrecht, Z. Galazka, J. Schwarzkopf, and A. Popp, AIP Adv. 11, 115323 (2021).
- [19] F. Alema, Y. Zhang, A. Mauze, T. Itoh, J. S. Speck, B. Hertog, and A. Osinsky, AIP Adv. **10**, 085002 (2020).
- [20] G. Seryogin, F. Alema, N. Valente, H. Fu, E. Steinbrunner, A. T. Neal, S. Mou, A. Fine, and A. Osinsky, Appl. Phys. Lett. **117**, 262101 (2020).
- [21] F. Alema, Y. Zhang, A. Osinsky, N. Orishchin, N. Valente, A. Mauze, and J. S. Speck, APL Mater. **8**, 021110 (2020).
- [22] F. Alema, G. Seryogin, A. Osinsky, and A. Osinsky, APL Mater. 9, 091102 (2021).
- [23] Z. Feng, A. F. M. Anhar Uddin Bhuiyan, M. R. Karim, and H. Zhao, Appl. Phys. Lett. 114, 250601 (2019).
- [24] Z. Feng, A. F. M. A. U. Bhuiyan, Z. Xia, W. Moore, Z. Chen, J. F. McGlone, D. R.
- Daughton, A. R. Arehart, S. A. Ringel, S. Rajan, and H. Zhao, Phys. Status Solidi RRL Rapid Res. Lett. **14**, 2000145 (2020).
- [25] L. Meng, Z. Feng, A. F. M. A. U. Bhuiyan, and H. Zhao, Cryst. Growth Des. 22, 3896 (2022).
- [26] A. Bhattacharyya, C. Peterson, T. Itoh, S. Roy, J. Cooke, S. Rebollo, P. Ranga, B. Sensale-Rodriguez, and S. Krishnamoorthy, APL Mater. 11, 021110 (2023).
- [27] L. Meng, A. F. M. A. U. Bhuiyan, Z. Feng, H.-L. Huang, J. Hwang, and H. Zhao, J. Vac. Sci. Technol. A 40, 062706 (2022).
- [28] A. F. M. A. U. Bhuiyan, Z. Feng, J. Johnson, Z. Chen, H.-L. Huang, J. Hwang, and H. Zhao, Appl. Phys. Lett. **115**, 120602 (2019).
- [29] A. F. M. A. U. Bhuiyan, Z. Feng, J. M. Johnson, H.-L. Huang, J. Sarker, M. Zhu, M. R. Karim, B. Mazumder, J. Hwang, and H. Zhao, APL Mater. **8**, 031104 (2020).
- [30] A. F. M. A. U. Bhuiyan, Z. Feng, L. Meng, and H. Zhao, J. Mater. Res. 36, 4804 (2021).
- [31] A. F. M. A. U. Bhuiyan, Z. Feng, L. Meng, A. Fiedler, H.-L. Huang, A. T. Neal, E.
- Steinbrunner, S. Mou, J. Hwang, S. Rajan, and H. Zhao, J. Appl. Phys. 131, 145301 (2022).
- [32] A. F. M. Anhar Uddin Bhuiyan, Z. Feng, J. M. Johnson, H.-L. Huang, J. Hwang, and H. Zhao, Cryst. Growth Des. **20**, 6722 (2020).
- [33] A. F. M. A. U. Bhuiyan, Z. Feng, J. M. Johnson, H.-L. Huang, J. Hwang, and H. Zhao, Appl. Phys. Lett. **117**, 142107 (2020).

- [34] A. F. M. A. Uddin Bhuiyan, L. Meng, H.-L. Huang, J. Sarker, C. Chae, B. Mazumder, J. Hwang, and H. Zhao, APL Mater. 11, 041112 (2023).
- [35] M.-Y. Tsai, O. Bierwagen, M. E. White, and J. S. Speck, J. Vac. Sci. Technol. A 28, 354 (2010).
- [36] P. Vogt and O. Bierwagen, Appl. Phys. Lett. 108, 072101 (2016).
- [37] M. Orita, H. Hiramatsu, H. Ohta, M. Hirano, and H. Hosono, Thin Solid Films 411, 134 (2002).
- [38] K. D. Leedy, K. D. Chabak, V. Vasilyev, D. C. Look, J. J. Boeckl, J. L. Brown, S. E. Tetlak, A. J. Green, N. A. Moser, A. Crespo, D. B. Thomson, R. C. Fitch, J. P. McCandless, and G. H. Jessen, Appl. Phys. Lett. **111**, 012103 (2017).
- [39] K. Matsuzaki, H. Hiramatsu, K. Nomura, H. Yanagi, T. Kamiya, M. Hirano, and H. Hosono, Thin Solid Films **496**, 37 (2006).
- [40] K. Nomura, K. Goto, R. Togashi, H. Murakami, Y. Kumagai, A. Kuramata, S. Yamakoshi, and A. Koukitu, J. Cryst. Growth **405**, 19 (2014).
- [41] H. Murakami, K. Nomura, K. Goto, K. Sasaki, K. Kawara, Q. T. Thieu, R. Togashi, Y. Kumagai, M. Higashiwaki, A. Kuramata, S. Yamakoshi, B. Monemar, and A. Koukitu, Appl. Phys. Express 8, 015503 (2014).
- [42] Y. Oshima, E. G. Villora, and K. Shimamura, Appl. Phys. Express 8, 055501 (2015).
- [43] S. Rafique, M. R. Karim, J. M. Johnson, J. Hwang, and H. Zhao, Appl. Phys. Lett. 112, 052104 (2018).
- [44] S. Rafique, L. Han, M. J. Tadjer, J. A. Freitas, N. A. Mahadik, and H. Zhao, Appl. Phys. Lett. **108**, 182105 (2016).
- [45] S. Saha, L. Meng, Z. Feng, A. F. M. Anhar Uddin Bhuiyan, H. Zhao, and U. Singisetti, Appl. Phys. Lett. **120**, 122106 (2022).
- [46] G. Wagner, M. Baldini, D. Gogova, M. Schmidbauer, R. Schewski, M. Albrecht, Z. Galazka, D. Klimm, and R. Fornari, Phys. Status Solidi A **211**, 27 (2014).
- [47] A. Fiedler, R. Schewski, M. Baldini, Z. Galazka, G. Wagner, M. Albrecht, and K. Irmscher, J. Appl. Phys. **122**, 165701 (2017).
- [48] R. Schewski, K. Lion, A. Fiedler, C. Wouters, A. Popp, S. V. Levchenko, T. Schulz, M. Schmidbauer, S. Bin Anooz, R. Grüneberg, Z. Galazka, G. Wagner, K. Irmscher, M. Scheffler, C. Draxl, and M. Albrecht, APL Mater. 7, 022515 (2019).
- [49] Z. Feng, A. F. M. A. U. Bhuiyan, Z. Xia, W. Moore, Z. Chen, J. F. McGlone, D. R. Daughton, A. R. Arehart, S. A. Ringel, S. Rajan, and H. Zhao, Phys. Status Solidi RRL Rapid Res. Lett. **14**, 2000145 (2020).
- [50] Z. Hu, K. Nomoto, W. Li, N. Tanen, K. Sasaki, A. Kuramata, T. Nakamura, D. Jena, and H. G. Xing, IEEE Electron Device Lett. **39**, 869 (2018).
- [51] W. Li, K. Nomoto, Z. Hu, D. Jena, and H. G. Xing, IEEE Electron Device Lett. 41, 107 (2020).
- [52] J. Yang, F. Ren, M. Tadjer, S. J. Pearton, and A. Kuramata, ECS J. Solid State Sci. Technol. 7, Q92 (2018).
- [53] S. Kumar, H. Murakami, Y. Kumagai, and M. Higashiwaki, Appl. Phys. Express 15, 054001 (2022).
- [54] P. Dong, J. Zhang, Q. Yan, Z. Liu, P. Ma, H. Zhou, and Y. Hao, IEEE Electron Device Lett. **43**, 765 (2022).
- [55] J.-S. Li, C.-C. Chiang, X. Xia, T. J. Yoo, F. Ren, H. Kim, and S. J. Pearton, Appl. Phys. Lett. **121**, 042105 (2022).

- [56] J. Zhang, P. Dong, K. Dang, Y. Zhang, Q. Yan, H. Xiang, J. Su, Z. Liu, M. Si, J. Gao, M. Kong, H. Zhou, and Y. Hao, Nat. Commun. **13**, 3900 (2022).
- [57] A. G. Thompson, Mater. Lett. **30**, 255 (1997).
- [58] C. A. Larsen, N. I. Buchan, S. H. Li, and G. B. Stringfellow, J. Cryst. Growth **102**, 103 (1990).
- [59] P. W. Lee, T. R. Omstead, D. R. McKenna, and K. F. Jensen, J. Cryst. Growth **85**, 165 (1987).
- [60] M. Pristovsek, M. Zorn, and M. Weyers, J. Cryst. Growth 262, 78 (2004).
- [61] J. L. Lyons, A. Janotti, and C. G. Van de Walle, Appl. Phys. Lett. 97, 152108 (2010).
- [62] N. Sawada, T. Narita, M. Kanechika, T. Uesugi, T. Kachi, M. Horita, T. Kimoto, and J. Suda, Appl. Phys. Express 11, 041001 (2018).
- [63] S. Mu, M. Wang, J. B. Varley, J. L. Lyons, D. Wickramaratne, and C. G. Van de Walle, Phys. Rev. B **105**, 155201 (2022).

Figure Captions

Figure 1. (a) Schematic of the SIMS sample with stacked sub-layers grown with different TMGa molar flow rate/growth rate. The growth temperature and chamber pressure were kept at 950 °C and 60 torr, respectively. The silane molar flow rate was set at 0.416 nmol/min for the Si-doped sub-layers. (b) The SIMS depth profiles of [C], [H], and [Si].

Figure 2. The extracted C, H and Si incorporation concentration as a function of the TMGa molar flow rate from the SIMS measurement of the sample as shown in Fig. 1.

Figure 3. (a) Measured free electron carrier concentration as a function of the silane molar flow rate for three different sets of samples varying the TMGa molar flow rate/growth rate. The dashed lines indicate the net compensation levels ([C]-[H]) for the three sets of samples grown at different growth rate. (b) Room temperature electron mobility as a function of carrier concentration for the three sets of samples grown with different TMGa molar flow rate/growth rate. The growth temperature and chamber pressure were kept at 950 °C and 60 torr, respectively.

Figure 4. (a) Schematic of the SIMS sample with stacked sub-layers grown with different temperature from 700 – 950 °C. The TMGa molar flow rate and chamber pressure were kept at 58 μmol/min and 60 torr, respectively. The silane molar flow rate was set at 0.416 nmol/min for the Si-doped sub-layers. (b) The SIMS depth profiles of [C], [H], and [Si].

Figure 5. The extracted C, H and Si incorporation concentration as a function of the growth temperature from the SIMS measurement of the sample as shown in Fig. 4.

Figure 1

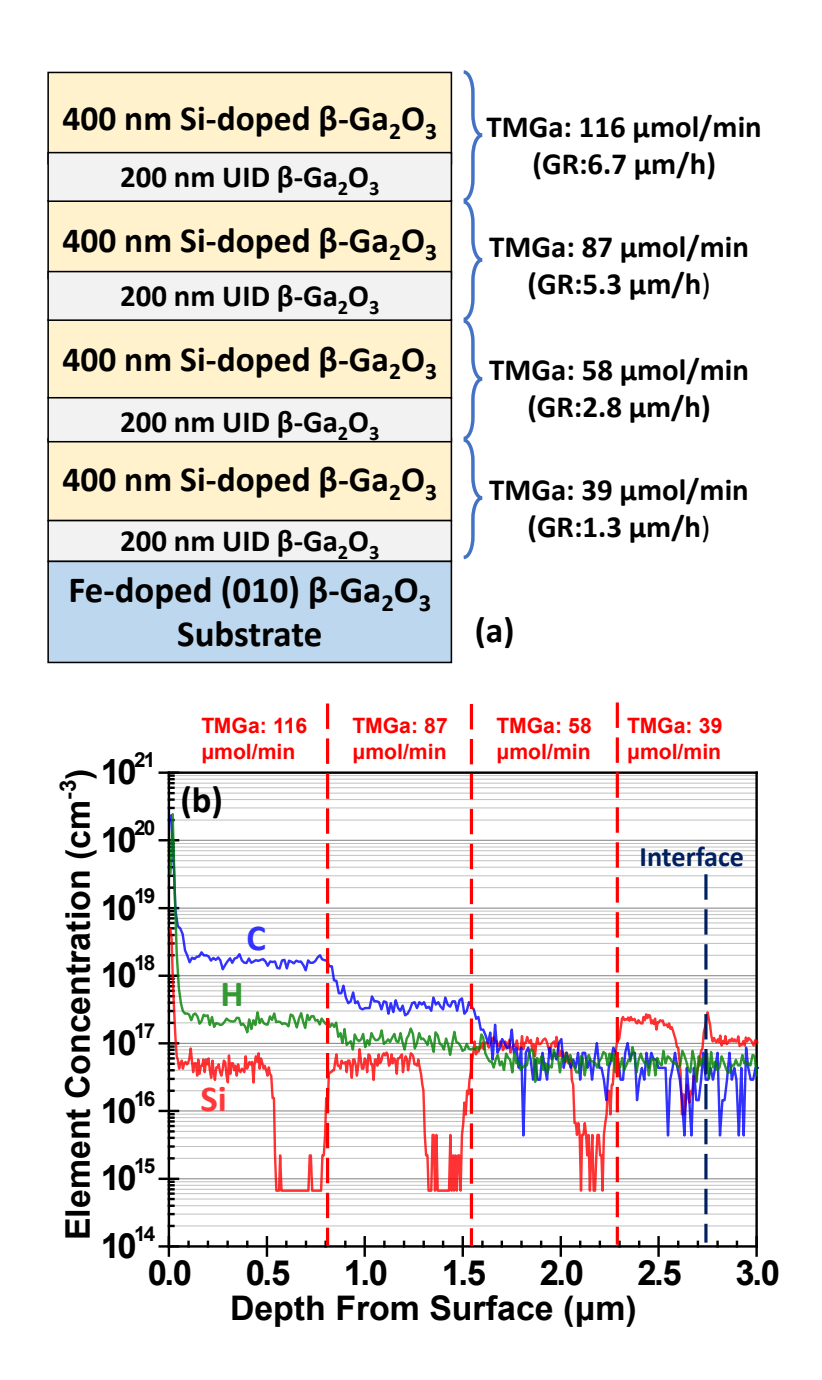


Figure 2

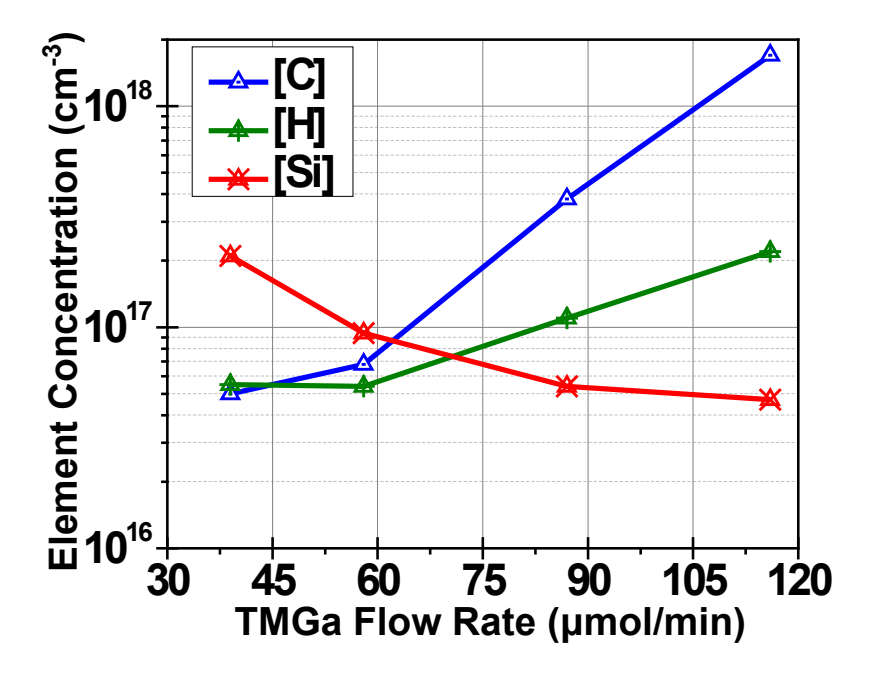
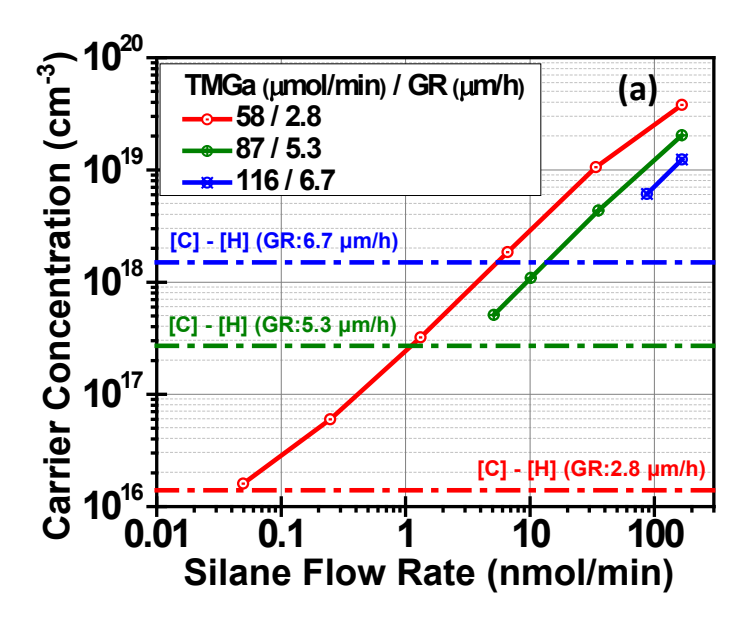


Figure 3



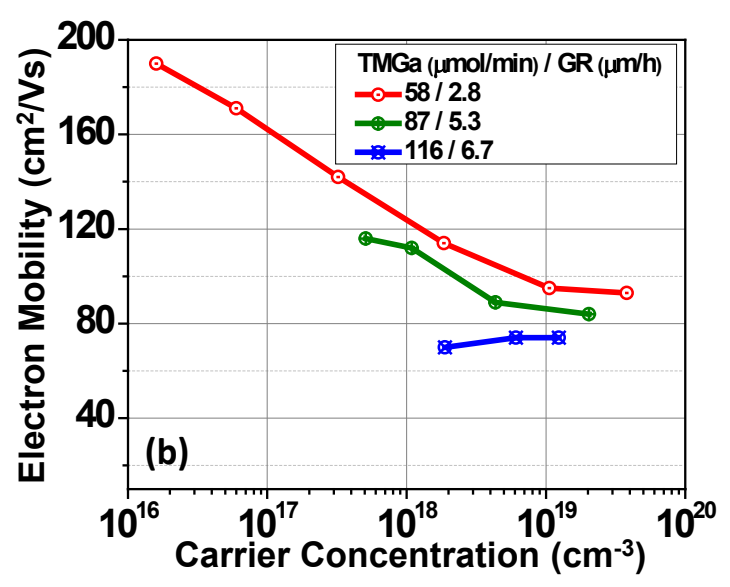
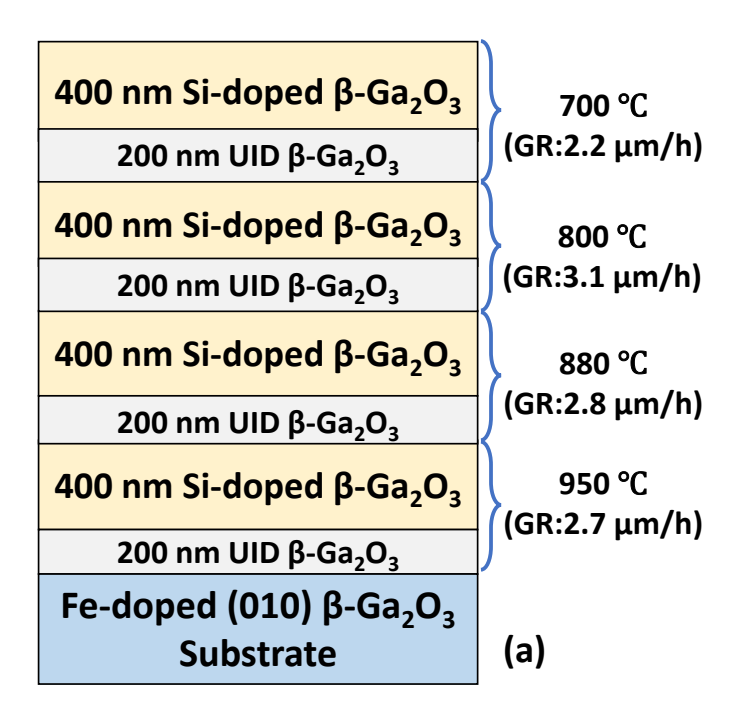


Figure 4



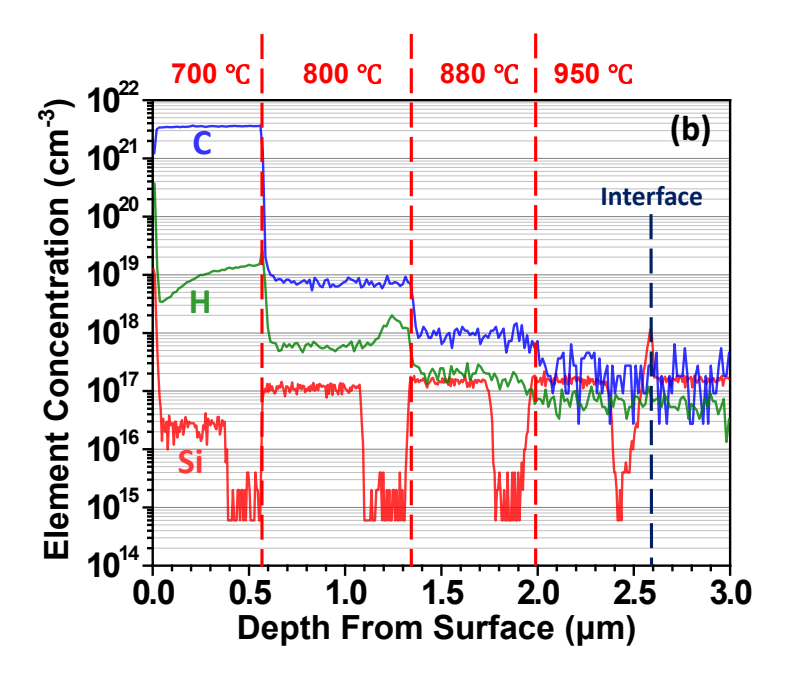


Figure 5

